Supporting Information

Improved stability of inverted and flexible perovskite solar cells with carbon electrode

Vivek Babu[1,2], Rosinda Fuentes Pineda[1], Taimoor Ahmad[1,2], Agustin O. Alvarez[3], Luigi Angelo Castriotta[2], Aldo Di Carlo[2], Francisco Fabregat-Santiago[3], Konrad Wojciechowski[1,4]*

[1] Saule Technologies, Wroclaw Technology Park, 11 Dunska Str., Sigma building, Wroclaw, PL 54-427, Poland

[2] University of Rome "Tor Vergata", CHOSE, Centre for Hybrid and Organic Solar Energy, Department Electronics Engineering, via del Politecnico 1, Roma, IT 00177, Italy

[3] University Jaume I, Institute of Advanced Materials, Avda. V. Sos Baynat s/n,

Castellon de la Plana, Castello, ES 12006, Spain

[4]Saule Research Institute, Wroclaw Technology Park, 11 Dunska Str., Sigma building,

Wroclaw, PL 54-427, Poland

*konrad.wojciechowski@sauletech.com

I.   EXPERIMENTAL SECTION

MATERIALS

All materials were used as received without purification as follows: lead iodide, PbI_2 (Sigma-Aldrich, 99.999%), lead bromide, $PbBr_2$ (Sigma-Aldrich, 98%), cesium iodide, CsI (Sigma-Aldrich, 99%), N,N-dimethylformamide, DMF (Sigma-Aldrich, anhydrous), dimethyl sulfoxide, DMSO (Sigma-Aldrich, anhydrous), toluene (Sigma-Aldrich, anhydrous), ethyl acetate (Sigma-Aldrich, anhydrous), chlorobenzene (Sigma-Aldrich, anhydrous), formamidinium iodide, FAI (Ajay North America), methylammonium bromide, MABr (synthesised in-house following the previously reported recipe)[1] , poly[bis(4-phenyl)(2,4,6-trimethylphenyl)aminePoly(triarylamine), PTAA (Osilla), (6,6)-phenyl C61 butyric acid methyl ester, PCBM (Lumtec), Tin (IV) oxide, SnO_2 (Alfa Aesar), poly(methyl methacrylate, PMMA (Sigma-Aldrich), carbon paste (DN-CP01 from Dyenamo).

DEVICE FABRICATION

p-i-n perovskite solar cell configuration: PET/IZO (Eastman, 15 Ω/□) substrates were cut (18x13 mm^2 pieces) and patterned by dipping one side in an HCl solution (15 wt.% in DI water). The etched substrates were cleaned by sonication in DI water (twice) and isopropanol for 5 minutes. The samples were then dried for 10 minutes on a hot plate at 100 °C, followed by 30 seconds of oxygen plasma treatment. PTAA solution was prepared by dissolving 2 mg of PTAA powder in 1 ml of toluene. A thin (~20 nm) PTAA layer was deposited under ambient conditions in a clean room by spin-coating at 5000 rpm for 30 seconds and then annealed at 100 ℃ for 10 minutes. Subsequently, the samples were transferred into a nitrogen-filled glovebox. The perovskite precursor solution composed of mixed cations and halides (final formula: $Cs_{0.04}(MA_{0.17}FA_{0.83})_{0.96}Pb(I_{0.83}Br_{0.17})_3$), dissolved in mixed solvents (DMF/DMSO = 4/1) was prepared according to the procedure reported before.[2] First, stock solutions of PbI_2 and $PbBr_2$ (1.5 mmol in 1 mL of DMF/DMSO 4:1 v/v) were prepared. These stock solutions were stirred at 180 °C for about 10 minutes, until all the powders were dissolved and clear looking solutions were obtained. The solutions were left to cool down to room temperature for around 20 minutes. To prepare the $FAPbI_3$

and MAPbBr$_3$ precursor solutions, MABr and FAI powders were weighed out into separate vials, and appropriate volumes of PbI$_2$ and PbBr$_2$ solutions were added to the respective vials to obtain an over stoichiometric lead content(FAI:PbI$_2$ and MABr:PbBr$_2$ yielding a molar ratio of 1:1.09). The solutions were stirred for 2-5 minutes until all the solids were fully dissolved. The final perovskite precursor solution was prepared by mixing together solutions of FAPbI$_3$ and MAPbBr$_3$ in a 5:1 v/v ratio. Then, CsI solution (36 μl of 1.5 M CsI solution in DMSO) was added to 1 ml of the aforementioned mixture. The polycrystalline perovskite layer was obtained by spin-coating the precursor solution on top of PTAA layer, using a two-step spinning program (1500 rpm for 2 seconds and 5000 rpm for 34 seconds). Anhydrous ethyl acetate (100 µL) was dispensed on the sample 10 seconds before the end of the spinning program. Then, the substrate was immediately transferred to the hotplate at 100 °C and annealed for 60 minutes. The electron transporting layer was deposited by spin-coating (2000 rpm for 30 seconds) a solution of PCBM:PMMA mixture (1 ml of 20 mg/ml PCBM solution per 30 μl of 10 mg/ml PMMA solution) in chlorobenzene. The layer was annealed for 10 minutes at 60 °C. Finally, 5 nm of Cr buffer layer and 100

nm of Ag electrode (optionally) were deposited on top of devices by thermal evaporation at ~10^{-6} bar, through a shadow mask. Carbon layer was blade-coated on top of the Cr layer and annealed with a heat gun. The substrate was placed on top of a polyoxymethylene plate for more localised heating.

n-i-p perovsktie solar cell configuration: PET/IZO (Eastman, 15 Ω/□) substrates were cut (18x13 mm^2 pieces) and patterned by dipping one side in an HCl solution (15 wt.% in DI water). The etched substrates were cleaned by sonication in DI water (twice) and isopropanol for 5 minutes. The samples were then dried for 10 minutes on a hot plate at 100 °C, followed by 30 seconds of oxygen plasma treatment. A 3% wt SnO_2 solution was prepared by diluting a 15% wt aqueous colloidal dispersion of SnO_2 in DI water A thin (~20 nm) SnO_2 layer was deposited under ambient conditions in a clean room by spin-coating at 2500 rpm for 30 seconds and then annealed at 100 ℃ for 30 minutes. Subsequently, the samples were transferred into a nitrogen-filled glovebox. The perovskite precursor solution was formulated exactly as mentioned in the previous section. The polycrystalline perovskite layer was obtained by spin-coating the precursor

solution on top of SnO$_2$ layer, using a two-step spinning program (1500 rpm for 2 seconds

and 5000 rpm for 34 seconds). Anhydrous ethyl acetate (100 µL) was dispensed on the

sample 10 seconds before the end of the spinning program. Then, the substrate was

immediately transferred to the hotplate at 100 °C and annealed for 60 minutes. For the

hole transporting layer , a PTAA solution (10 mg/mL in toluene) was prepared with

dopants including bis(trifluoromethylsulfonyl)imide lithium salt (Li-TFSI) (17 µl ml−1 of a

170 mg ml−1 solution in acetonitrile) and 4-*tert*-butylpyridine (*t*BP, 28.8 µl ml−1). The layer

was formed by spin coating PTAA solution at 3000 rpm for 30 seconds. Finally, 5 nm of

Cr buffer layer was deposited on top of devices by thermal evaporation at ~10^{-6} bar,

through a shadow mask. Carbon layer was blade-coated on top of the Cr layer and

annealed with a heat gun. The substrate was placed on top of a polyoxymethylene plate

for more localised heating.

DEVICE CHARACTERISATION

Current density–voltage characterization and stabilized power output measurements were performed using a Keithley 2461 source measure unit (SMU) under simulated AM1.5G irradiation (100 mA cm^{-2}) using an AAA-rated solar simulator (Abet Technologies, sun 2000) calibrated against an RR-208-KG5 silicon reference cell (Abet Technologies). The mismatch factor for the studied perovskite solar cells was calculated to be 0.96 (using EQEs of the reference and test cells, lamp's spectrum, and AM1.5G), and this value was used correct the intensity of the solar simulator lamp to provide one sun illumination.[3] Solar cells were masked to 1 cm^2. JV measurements were performed in in two scan directions, from forward bias to short-circuit and from short-circuit to forward bias. The scanning rate was set to 0.5 V s−1. The stabilized power conversion efficiency (SPO) was measured at the maximum power point voltage for a duration of 30 seconds. The EQE was measured using Bentham PVE300 photovoltaic characterization system and the control software BenWin+.

Electrochemical impedance spectroscopy (EIS) measurements were done using an Autolab PGSTAT204 equipped with a FRA32M EIS module. The bias potentials were ranged between 0 and 1 V under high intensity LED illumination. To enable comparisons, the same potentials were applied in dark and under illumination, same for all the studied cells. A 20 mV AC perturbation was applied ranging between 1 MHz and 100 mHz. To avoid degradation and have a controlled atmosphere during the measurements, they were carried out in a dry box, with less than 0.1% RH.

The transient photovoltage (TPV) and transient photocurrent (TPC) were measured with a commercial apparatus (Arkeo, Cicci Research s.r.l.) based on a high-speed Waveform Generator that drives a high speed LED (5000 Kelvin). The device is connected to a transimpedance amplifier and a differential voltage amplifier to monitor short-circuit current or open-circuit voltage. The measurements were executed with varied light intensities. The intensities were cycled at 10 different levels (from 30 mW.cm^{-2} up to 160 mW.cm^{-2}), using the white LED. For each intensity level, 200 traces were recorded.

II.   ADDITIONAL DATA
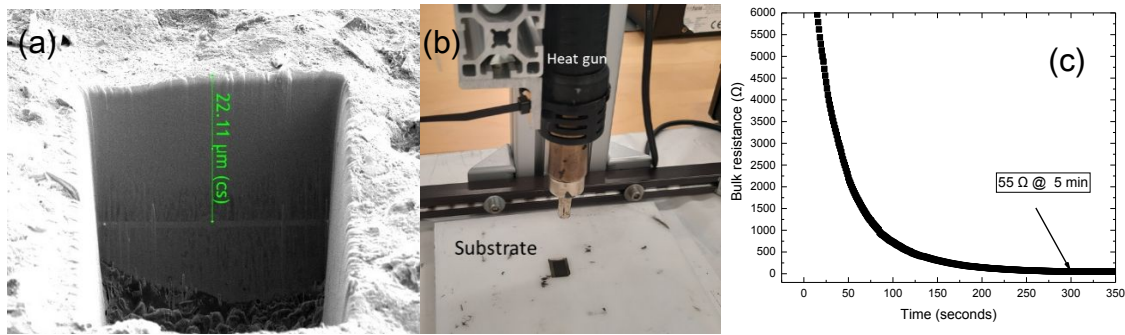
Figure S1. (a) Cross-section FIB-SEM image of the 20 µm thick carbon layer; (b) photo

of a gas blowing setup for annealing carbon films; (c) resistance of a blade-coated carbon

film plotted as a function of annealing time.
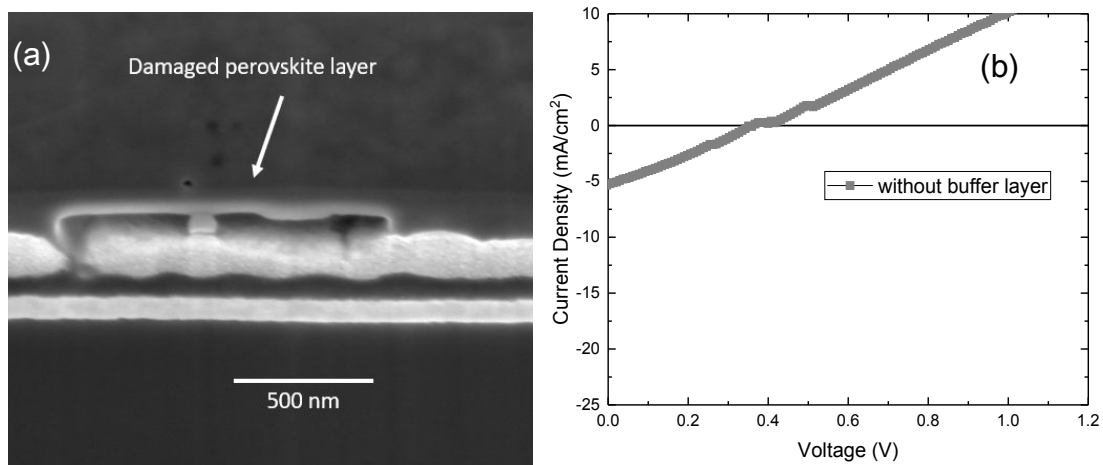
Figure S2. (a) Cross-section FIB-SEM image of a p-i-n perovskite solar cell with carbon

back contact electrode (no buffer layer), displaying mechanical damage in the perovskite

layer; (b) current density – voltage curve of such solar cell showing a shunted

characteristic.
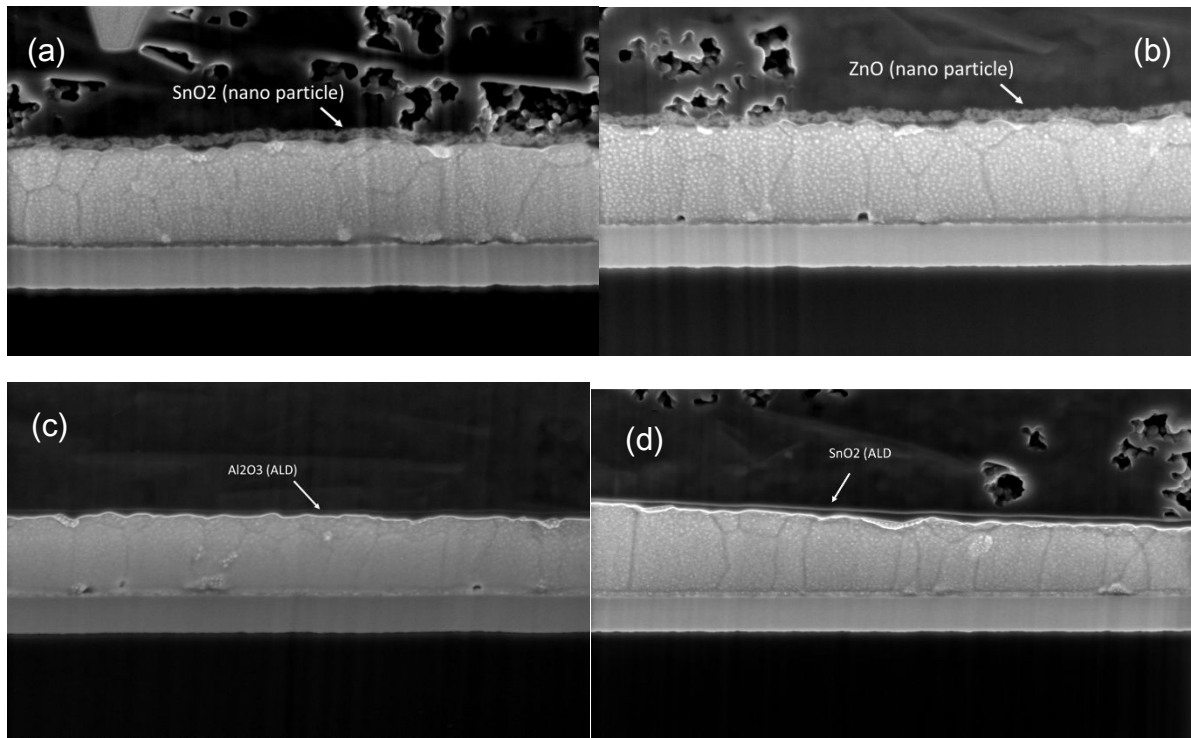
Figure S3. Cross-section FIB-SEM images of p-i-n carbon devices with different buffer layers: (a) SnO_2 nanoparticles; (b) ZnO nanoparticles; (c) Al_2O_3 (deposited by ALD); (d) SnO_2 (deposited by ALD).

Figure S4. Picture of a p-i-n perovskite solar cell with the Cr/C back contact electrode, deposited on a flexible substrate.
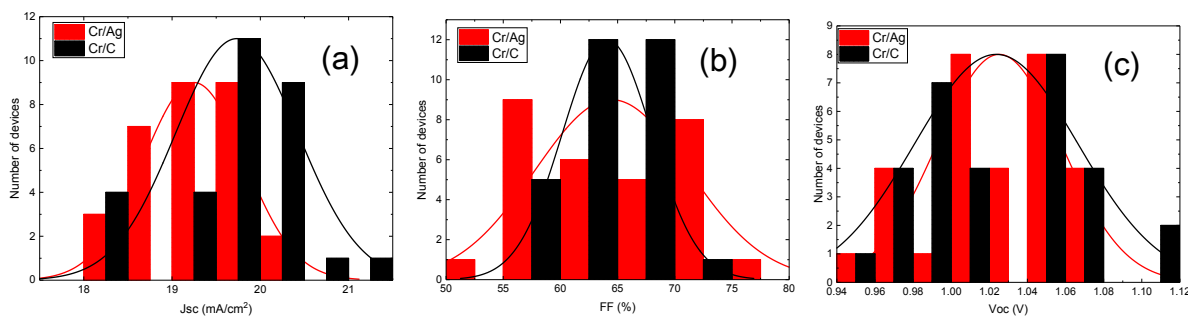

Figure S5. Histograms of photovoltaic parameters extracted from JV measurements of perovskite solar cells (30 individual cells) of p-i-n configuration, with the Cr/C and Cr/Ag back electrode types, (a) short-circuit current density, (b) fill factor, (c) open-circuit voltage.

Table S1. Detailed information on the statistics of photovoltaic parameters extracted from

JV measurements of perovskite solar cells of p-i-n configuration, with the Cr/C and Cr/Ag

back electrode types.

| Cr_C						
Data	N total	Mean	Standard Deviation	Minimum	Median	Maximum
Efficiency [%]	30	12.94	0.99	11.03	12.84	15.18
Fill Factor [%]	30	64.08	3.94	56.13	64.09	71.14
V_OC [V]	30	1.02	0.04	0.96	1.01	1.10
J_SC [mA/cm²]	30	19.73	0.69	18.33	19.84	21.18
Cr_Ag						
Data	N total	Mean	Standard Deviation	Minimum	Median	Maximum
Cr_Ag						
Efficiency [%]	30	12.72	1.69	10.25	12.49	15.71
Fill Factor [%]	30	64.48	6.72	53.23	64.87	77.1
V_OC [V]	30	1.03	0.03	0.95	1.03	1.07
J_SC [mA/cm²]	30	19.25	0.57	18.13	19.24	20.35
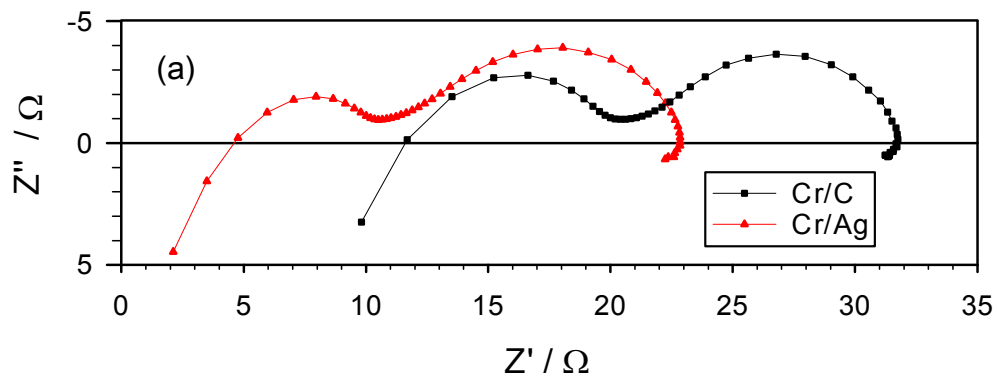
(b)
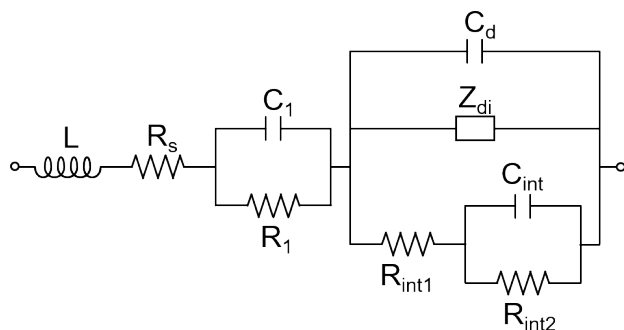
Figure S6. (a) Nyquist plots obtained for the IS measurements (illumination, applied

voltage close to V_{OC}) of perovskite solar cells with the Cr/C and Cr/Ag electrode types;

(b) proposed equivalent circuit model.

To analyse the impedance response, we propose the equivalent circuit shown in Figure

S6b, which is based on the previously proposed models.[4-6] The first element is an inductor

(L) and it is related with wires and connection effects observable at high frequencies,

responsible for the high frequency Z'-axis crossing. The second element, the most

important for the present analysis, is the series resistance (R_{series}) which mainly includes

the combination of resistive contributions from connections and transport resistances in

the bulk of carrier transporting layers, including ITO, carbon, silver, and also charge

selective layers. This element is related to the high frequency limit of Z'. After that, there

S14

is an RC in parallel (R_1 and C_1), generating the first arc in the IS response, related to the

charge transfer, charge transport, and charge accumulation properties at selective layers

and their interfaces. Following that RC, there is a more complex combination of elements

that is related to the perovskite behaviour. It includes resistances associated with the

transport and recombination in the perovskite layer (R_{int1}, R_{int2}), the interfacial capacitance

of perovskite (C_{int}), which also includes ionic and electronic accumulation capacitances,

the dielectric capacitance of perovskite (C_d) and the diffusion element (Z_{di}) accounting for

ionic contribution to the electrical response.[7] This combination of elements is associated

with the second deformed arc, because these are different processes occurring with

similar time constant.

Table S2. Photovoltaic parameters corresponding to JV curves from Figure 3a, which

were calculated by removing the series resistance (Rseries) contribution from the JV

curves (reverse scan direction) shown in Figure 2a.

PIN		PCE [%]	FF [%]	Jsc [mA/cm^2]	V$_{OC}$ [V]
Cr/Carbon	RS	17.14	77.22	21.11	1.05
Cr/Silver	RS	15.92	77.71	20.13	1.01
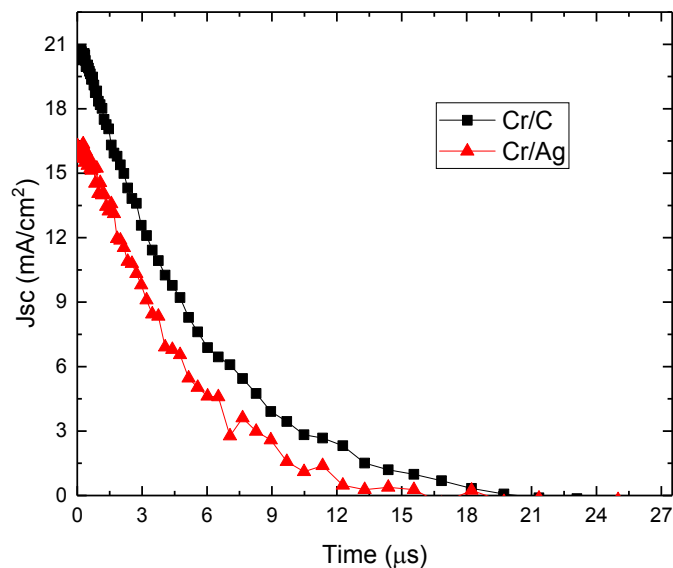
Figure S7. Photocurrent density decay plots for perovskite solar cells with the Cr/C and

Cr/Ag electrode types, measured at the excitation light intensity corresponding to 1.5 sun.\
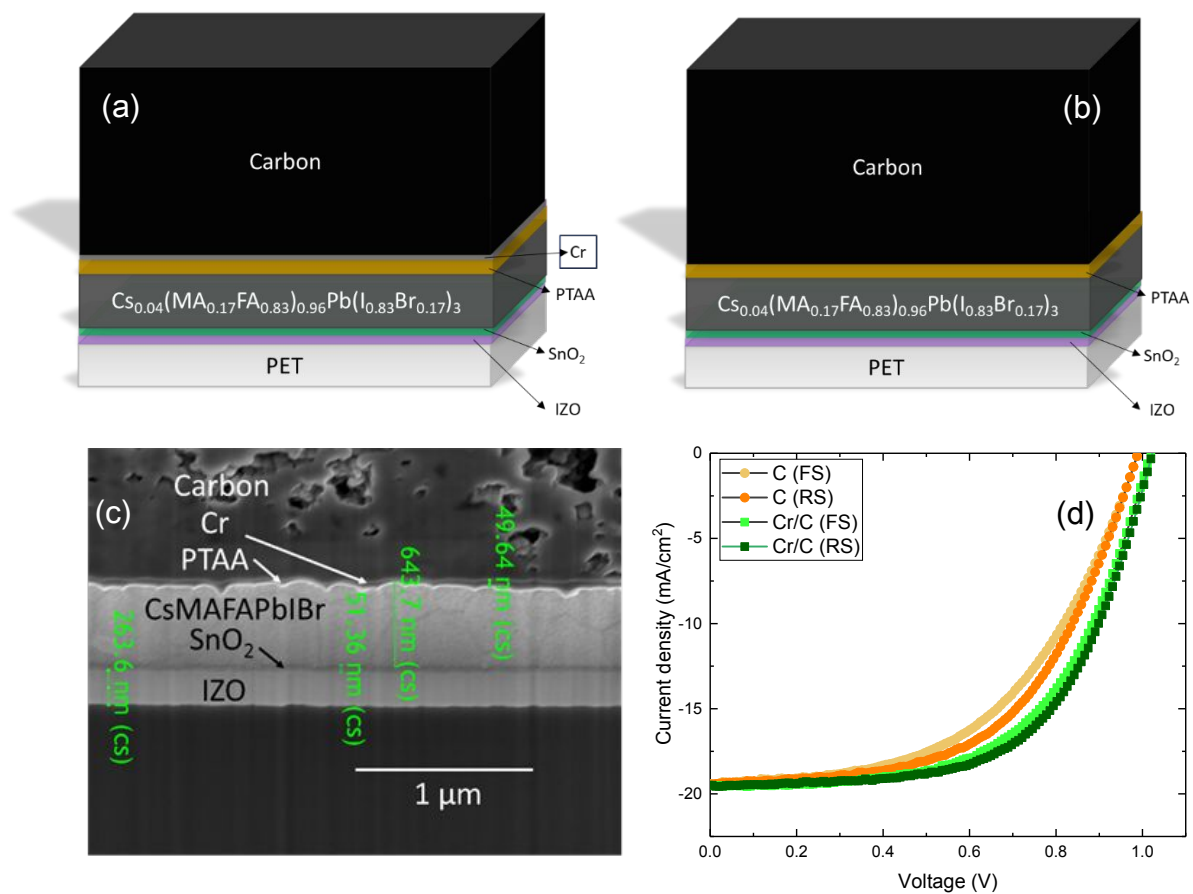
Figure S8. Schematics of carbon-based n-i-p device structures, (a) with Cr interlayer, and

(b) without; (c) cross-section FIB-SEM image of the perovskite solar cell of n-i-p

configuration with the Cr buffer layer; (d) JV characteristics of n-i-p perovskite solar cells

(with and without Cr buffer layer), in forward (FS) and reverse (RS) scan directions.

Table S3. Photovoltaic parameters of Cr /C and Cr /Ag devices under reverse (RS) and

forward (FS) scan directions.

| NIP		PCE [%]	FF [%]	Jsc [mA/cm^2]	V_{OC} [V]
Cr/C	FS	11.57	58.67	19.5	1.01
	RS	12.06	60.72	19.5	1.02
C	FS	9.95	51.94	19.43	0.99
	RS	10.68	55.64	19.43	0.99
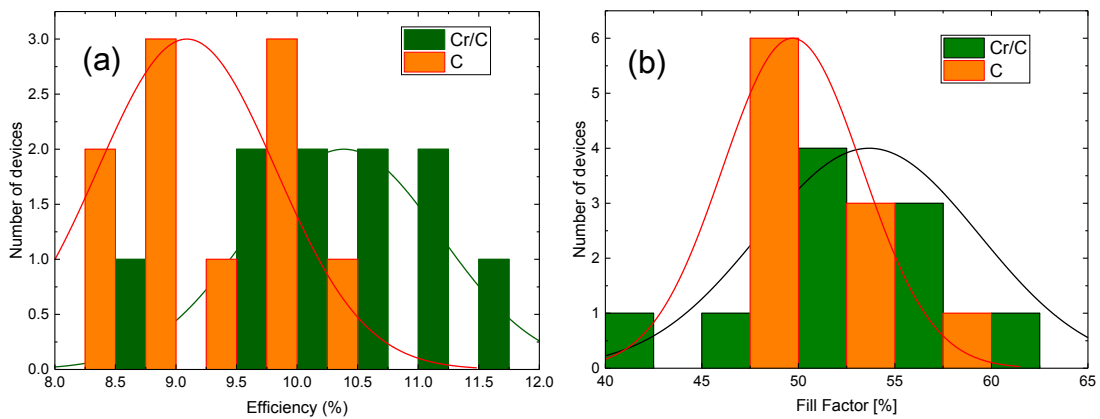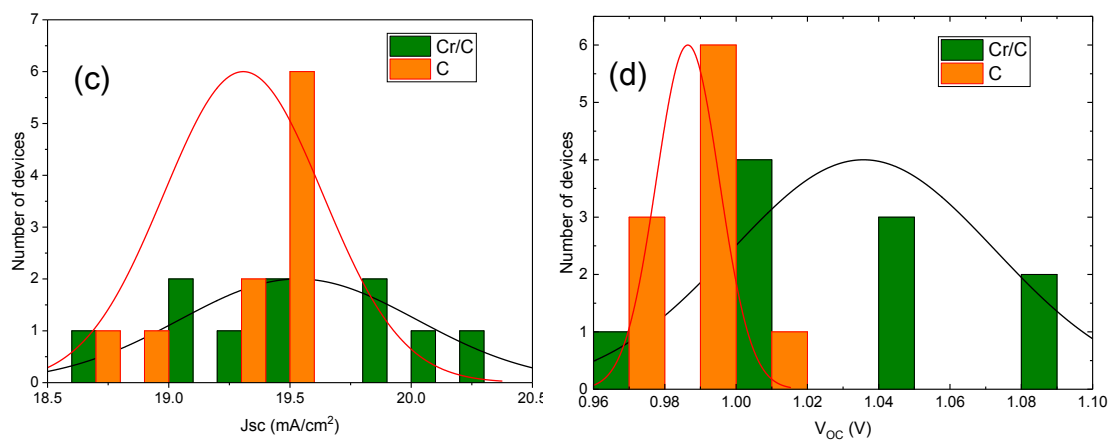
Figure S9. Histograms of photovoltaic parameters extracted from JV measurements of carbon-based perovskite solar cells (30 individual cells) of n-i-p configuration, with and without Cr buffer layer, (a) efficiency, (b) fill factor, (c) short-circuit current density, (d) open-circuit voltage.

Table S4. Detailed information on the statistics of photovoltaic parameters extracted from JV measurements of perovskite solar cells of n-i-p configuration, with and without Cr buffer layer.

NIP_Cr/C

Data	N total	Mean	Standard Deviation	Minimum	Median	Maximum
Efficiency [%]	10	10.82	0.83	9.18	10.90	12.06
Fill Factor [%]	10	53.67	5.71	42.29	53.86	60.72
V_OC [V]	10	1.04	0.04	0.97	1.03	1.09
I_SC [mA]	10	19.53	0.49	18.72	19.50	20.26
NIP_C						
Data	N total	Mean	Standard Deviation	Minimum	Median	Maximum
Efficiency [%]	10	9.47	0.77	8.48	9.40	10.68
Fill Factor [%]	10	49.69	3.62	45.19	48.86	55.64
V_OC [V]	10	0.99	0.01	0.97	0.99	1.00
I_SC [mA]	10	19.31	0.33	18.61	19.43	19.59
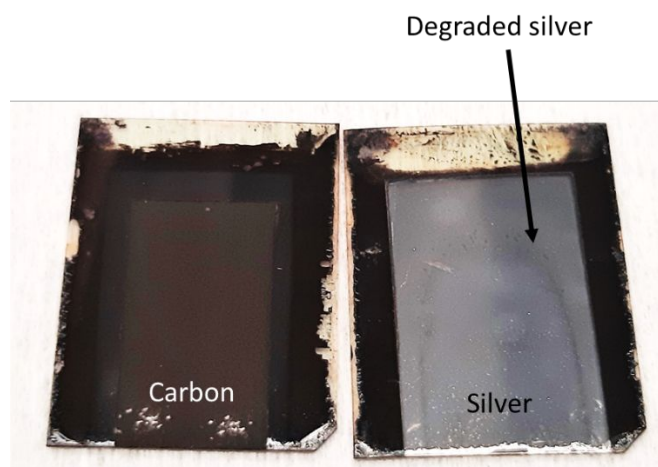
Figure S10. Photography of perovskite solar cells with the Cr/C (left) and Cr/Ag (right)

electrode types, taken after 1000 hours of thermal test at 85 °C. Observed visual changes

in the silver layer was marked.

REFERENCES

(1)   Singh, R. K.; Kumar, R.; Kumar, A.; Jain, N.; Singh, R. K.; Singh, J. Novel Synthesis Process of Methyl Ammonium Bromide and Effect of Particle Size on Structural, Optical and Thermodynamic Behavior of CH3NH3PbBr3 Organometallic Perovskite Light Harvester. *J. Alloys Compd.* **2018**, *743*, 728–736. https://doi.org/10.1016/j.jallcom.2018.01.355.

(2)   Saliba, M.; Correa-Baena, J. P.; Wolff, C. M.; Stolterfoht, M.; Phung, N.; Albrecht, S.; Neher, D.; Abate, A. How to Make over 20% Efficient Perovskite Solar Cells in Regular (n-i-p) and Inverted (p-i-n) Architectures. *Chem. Mater.* **2018**, *30*, 4193–4201. https://doi.org/10.1021/acs.chemmater.8b00136.

(3)   Shrotriya, V.; Li, G.; Yao, Y.; Moriarty, T.; Emery, K.; Yang, Y. Accurate Measurement and Characterization of Organic Solar Cells. *Adv. Funct. Mater.* **2006**, *16*, 2016–2023. https://doi.org/10.1002/adfm.200600489.

(4)   García-Fernández, A.; Moradi, Z.; Bermúdez-García, J. M.; Sánchez-Andújar, M.;

Gimeno, V. A.; Castro-García, S.; Senarís-Rodríguez, M. A.; Mas-Marzá, E.; Garcia-Belmonte, G.; Fabregat-Santiago, F. Effect of Environmental Humidity on the Electrical Properties of Lead Halide Perovskites. *J. Phys. Chem. C* **2019**, *123*, 2011–2018. https://doi.org/10.1021/acs.jpcc.8b03915.

(5)   Ravishankar, S.; Aranda, C.; Sanchez, S.; Bisquert, J.; Saliba, M.; Garcia-Belmonte, G. Perovskite Solar Cell Modeling Using Light- and Voltage-Modulated Techniques. *J. Phys. Chem. C* **2019**, *123*, 6444–6449. https://doi.org/10.1021/acs.jpcc.9b01187.

(6)   Zarazua, I.; Han, G.; Boix, P. P.; Mhaisalkar, S.; Fabregat-Santiago, F.; Mora-Seró, I.; Bisquert, J.; Garcia-Belmonte, G. Surface Recombination and Collection Efficiency in Perovskite Solar Cells from Impedance Analysis. *J. Phys. Chem. Lett.* **2016**, *7*, 5105–5113. https://doi.org/10.1021/acs.jpclett.6b02193.

(7)   Li, C.; Guerrero, A.; Huettner, S.; Bisquert, J. Unravelling the Role of Vacancies in Lead Halide Perovskite through Electrical Switching of Photoluminescence. *Nat.*

Commun. **2018**, *9*, 5113. https://doi.org/10.1038/s41467-018-07571-6.